NANOSYSTEMS: PHYSICS, CHEMISTRY, MATHEMATICS, 2015, 6 (6), P. 866–874

Crystallization behavior and morphological features of $YFeO_3$ nanocrystallites obtained by glycine-nitrate combustion

V. I. Popkov[1,3], O. V. Almjasheva[2,3], V. N. Nevedomskiy[3], V. V. Sokolov[3], V. V. Gusarov[1,2,3]

[1] Saint Petersburg State Technological Institute (Technical University), 190013, St. Petersburg, Moskovsky prospect 26

[2] Saint Petersburg Electrotechnical University "LETI", 197376, St. Petersburg, Professora Popova str. 5

[3] Ioffe Physical Technical Institute, 194021, St. Petersburg, Politekhnicheskaya str. 26

vadim.i.popkov@gmail.com, almjasheva@mail.ru

PACS 61.46.+w **DOI 10.17586/2220-8054-2015-6-6-866-874**

Yttrium orthoferrite nanocrystallites with hexagonal and orthorhombic structures were obtained directly by the glycine-nitrate synthesis. The nanocrystallites have plate-like morphology and are strongly agglomerated in highly-porous structures, as was shown by the TEM investigation. The influences of the synthesis conditions on the yttrium orthoferrite crystallization, its nanocrystallite size and morphology are discussed.

Keywords: yttrium orthoferrite, $YFeO_3$, glycine-nitrate combustion, nanoparticles.

Received: 30 October 2015

Revised: 2 November 2015

1. Introduction

Direct solution combustion synthesis of oxide nanoparticles is of great interest currently because of its rapidity, simplicity and cost effectiveness [1–13]. Nanoparticles obtained by this method, as a rule, possess comparatively narrow size distribution and high surface area [5–7], which provides the possibility for its industrial and technical use. In some cases, combustion products may take on the role of precursors for obtaining new nanostructures of another principal morphology, structure and surface state [14–16]. This and other factors have led to an increased number of research efforts having been dedicated to combustion synthesis in recent years.

Yttrium orthoferrite is the one of the most interesting representatives of the complex oxide multiferroics – materials that are both ferroelectric and magnetic. Previously, this compound had been obtained in a nanostructured state by a number of so-called 'soft-chemical' methods [17–23], including combustion methods [24–28]. Despite the successful synthesis of yttrium orthoferrite nanoparticles from different initial solutions, it should be noted that data about processes leading to $YFeO_3$ nanosized particle formation as well as about influence of synthetic conditions on its results are quite limited.

The present paper is an expansion of the investigations which were initiated previously [26–28] and aims to obtain detailed information about the interrelation between synthetic conditions, composition, structure, dispersity and properties of yttrium orthoferrite nanoparticles, obtained by glycine-nitrate combustion. This work will accomplish this by analyzing the phase composition, crystallinity and morphology features of yttrium orthoferrite nanocrystallites formed under combustion.

2. Experimental

2.1. Synthesis procedure

Yttrium orthoferrite nanocrystallites were obtained by combustion of a glycine-nitrate precursor with the glycine to total yttrium and iron nitrates ratio equal to 2.4, 3.0, 3.3, 3.6 and 4.2. This procedure was described in detail previously in work [26].

Glycine H_2NCH_2COOH (p.a.) was added in the required ratio to a solution of iron (III) nitrate $Fe(NO_3)_3$ (pur.) and yttrium nitrate $Y(NO_3)_3$ (puriss.), taken in equimolar amounts. The resulting solution changed the color to dark brown due to the formation of glycine complex with metal cations. Then, the solution was heated until complete water evaporation and then self-ignition occurred that resulted in formation of brown fluffy powder.

Then products of glycine-nitrate combustion were calcined at 800 °C for 15 minute to remove impurities associated with incomplete combustion products, predominantly consisting of carbon black.

2.2. Characterization of the prepared samples

The elemental composition of the specimens was analyzed by means of scanning electron microscopy (SEM) using a Hitachi S-570, coupled with Oxford Link Pentafet microprobe analyzer.

The phase composition of the specimens were controlled by powder X-ray diffraction (XRD) using a Shimadzu XRD-7000 with monochromatic CuKα radiation ($\lambda = 0.154051$ nm). Qualitative X-Ray analysis was carried out with powder base of the diffraction data PDF2-2012 using, quantitative X-Ray analysis was carried out with using of the Rietveld method [29]. Average crystallite size for spherical nanoparticles was calculated according to Scherer's formula [30]:

$$D = \frac{0.9 \cdot \lambda}{\beta \cdot \cos(\theta)},$$

where λ – X-ray wavelength, β – full width at half-maximum, θ – Bragg angle.

Specific surface areas were determined with Micromeritics ASAP 2020 by the BET method using nitrogen as the adsorbant. Pycnometric densities were measured with using Micromeritics AccuPyc 1330 helium pycnometer. Average wall thickness of the pores was estimated using the formula for an infinite plate of finite thickness, by which in the first approximation, we described the morphology of the system:

$$h = \frac{2}{S \cdot \rho},$$

where h – average wall thickness of the pores, S – specific surface area and ρ – density of the sample.

Transmission electron microscopy (TEM) image was taken on a JEOL TEM-100CX transmission electron microscope.

3. Results and discussion

Results of elemental analysis for compositions obtained after glycine-nitrate combustion showed that molar ratio Fe:Y equels to stoichiometric value for all the samples in the range of the method error [31] (Table 1).

According to the results of XRD analysis (Fig. 1), the phase composition of the combustion products strongly depends on the G/N ratio of the initial solution.

TABLE 1. X-ray microanalysis results of the glycine-nitrate combustion products

G/N	Fe:Y molar ratio, %	
	X-ray microanalysis	**Synthesis**
2.4	51.0:49.0	50:50
3.0	50.4:48.6	
3.3	51.3:48.7	
3.6	49.4:50.6	
4.2	50.8:49.2	

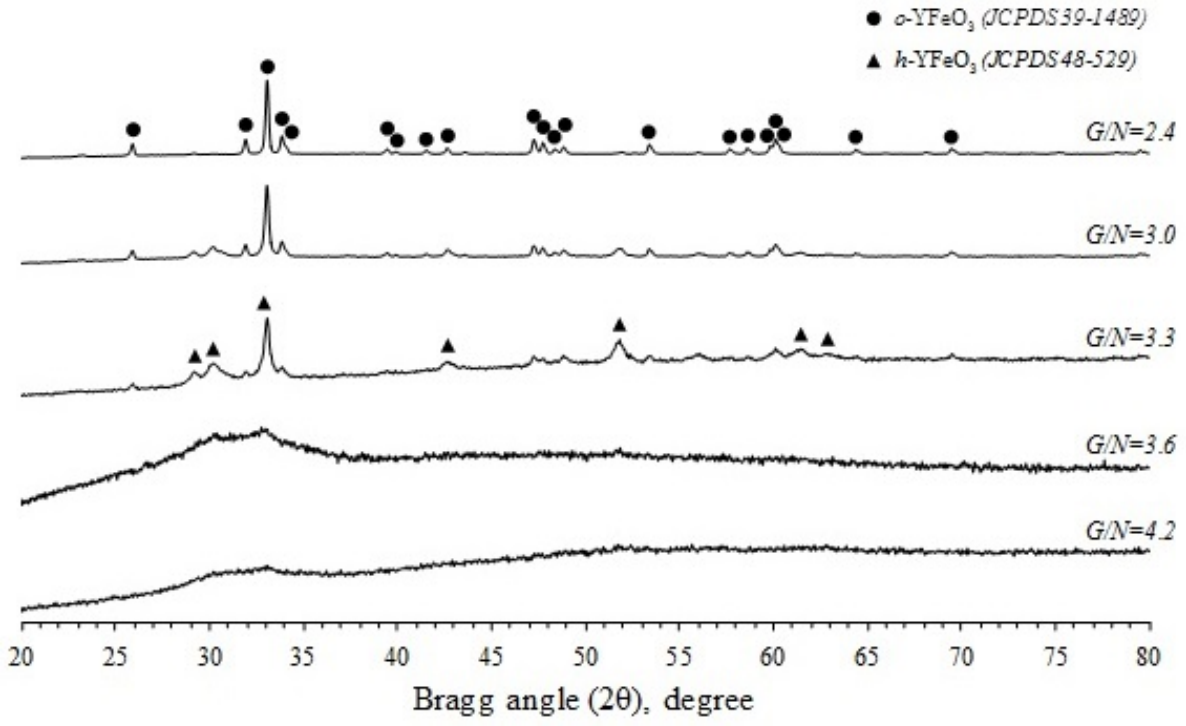

FIG. 1. XRD patterns of glycine-nitrate combustion products obtained at different G/N ratio

As one can observe, samples obtained at a glycine to nitrate ratio equal to 3.6 and 4.2 are X-ray amorphous. However with glycine molar fraction increasing, hexagonal (h-$YFeO_3$) and orthorhombic yttrium ferrite (o-$YFeO_3$) phase appearaences are observed in XRD patterns samples. Finaly at a G/N ratio of 2.4, the sample almost completely consists of stable o-$YFeO_3$ phase. The possible reasons for the considered system's behavior were discussed in earlier works [26, 27] as well as the amorphous, hexagonal and orthorhombic phases' relations to their synthesis by glycine-nitrate combustion processes.

On the basis of XRD results, quantitative phase and disperse composition of the samples were obtained (Table 2). Additional data about pycnometric density and specific surface area are also shown.

TABLE 2. Phase and disperse compositions, pycnometric density and specific surface area of glycine-nitrate combustion products

G/N	Mole fraction, %			Average crystallite size, nm		Pycnometric density, g/cm^3	Specific surface area, m^2/g
	***o*-$YFeO_3$**	***h*-$YFeO_3$**	**amorphous phase**	***o*-$YFeO_3$**	***h*-$YFeO_3$**		
2.4	95.4	4.6	0	49±5	< 7	5.3544	5.8
3.0	46.3	42.7	11.0	42±4		5.0627	27.0
3.3	12.9	48.3	38.8	31±3		4.2964	35.0
3.6	0	0	100	–	–	3.5366	24.8
4.2	0	0	100	–	–	2.9045	14.8

As it is shown in Table 2, the pycnometric density of the samples decreases with an increasing of amorphous phase mole fraction, which consist of amorphous $YFeO_3$ as well as of incomplete combustion products and absorbed water [28]. But even for a sample with G/N ratio of 2.4, its pycnometric density is quite far from X-ray densities for pure hexagonal and orthorhombic phases – 5.526 and 6.195 g/cm^3 respectively. This can be explained by the presence of closed porosity in the samples which can reach values of 30 % and higher.

The dependence of specific surface area upon the glycine/nitrates ratio is more complicated and has maximum (about 35 m^2/g) at G/N ratio equal to 3.3. This may be explained by decisive contribution of the hexagonal ultradisperse $YFeO_3$ phase in total surface area. Thus, in the G/N ratio range of 2.4 – 3.3 increasing of hexagonal $YFeO_3$ mole fraction causes an increase in the specific surface area of the sample. It should be noted that for the X-ray amorphous samples ($G/N = 3.6$ and 4.2) the observed total surface area decrease with higher G/N ratio may be due to the fouling of surface and porous structure by incomplete combustion products under conditions of excess glycine.

Compositions obtained by the glycine-nitrate combustion were then calcined at 800 °C for 15 minutes, which resulted in its significant weight loss and formation of monophasic samples of orthorhombic yttrium ferrite for all G/N ratios. Relative weight loss of the samples and average crystallite sizes of *o*-$YFeO_3$ depending on glycine to nitrates ratio in initial solution are shown in Fig. 2.

As one can see, the maximum weight loss after calcination is constant for the samples with high glycine excess toward its stoichiometric amount and reaches about 20 % for $G/N = 4.2$. Weight loss decreases monotonically with a decreasing glycine to nitrate ratio and for the sample with $G/N = 2.4$, it is comparable with accuracy of the used method. Thus, it can be concluded that in the case of a slight glycine deficiency toward reaction stoichiometry, it is possible to obtain nanocrystalline pure phase of orthorhombic yttrium orthoferrite by direct glycine-nitrate combustion without the necessity of additional thermal treatment.

Average crystallite size of orthorhombic $YFeO_3$ obtained after calcination of combustion products considerably changes from 30 to 50 nm with G/N ratio change from 4.2 to 2.4. Wherein this dependence upon G/N has two characteristic ranges – for G/N from 4.2 – 3.3, calcination of products leads to the formation of relatively smaller nanoparticles than in case of G/N equal to 3.3 – 2.4. This may be considered as result of presence a carbon skeleton

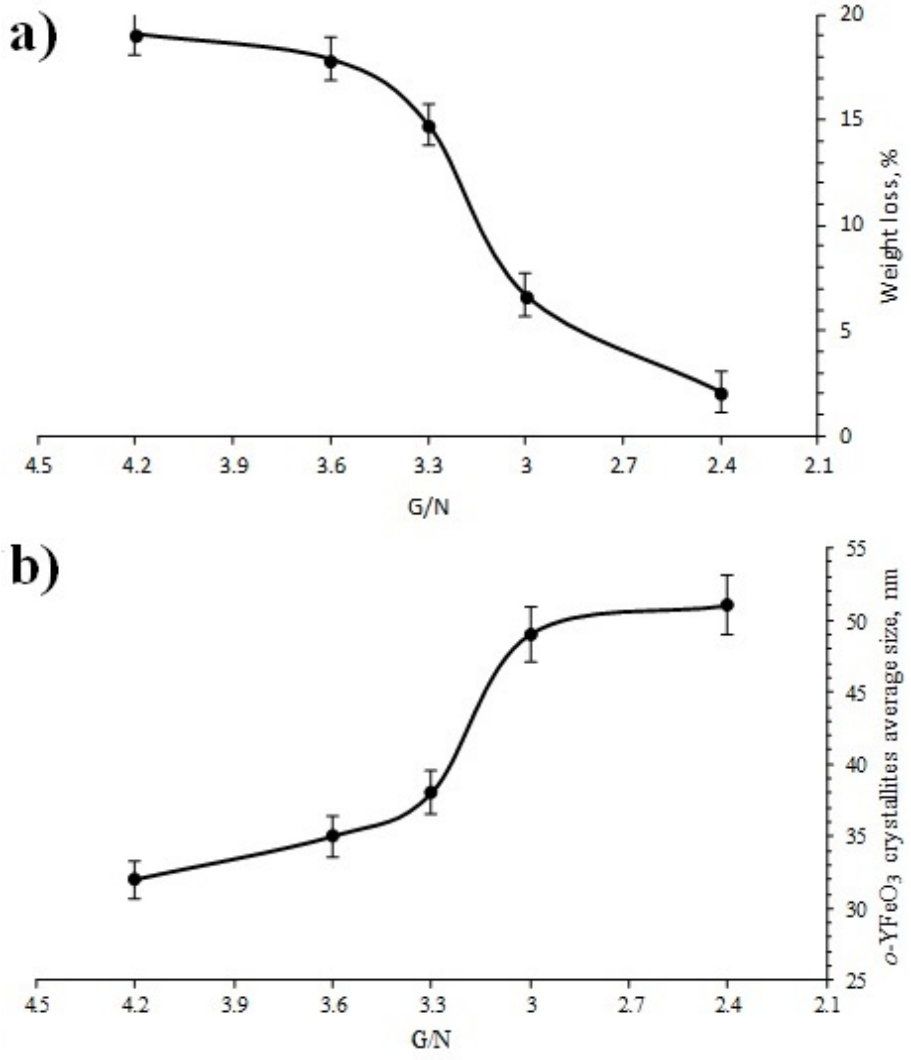

FIG. 2. Relative weight loss (a) and average *o*–$YFeO_3$ crystallites size (b) after calcination of glycine-nitrate combustion products at 800 °C for 15 minutes

in the samples obtained under conditions of glycine excess. This, in turn, leads to spatial separation of nanoparticles formed under thermal treatment of combustion products and restricts recrystallization processes. In the absence of a carbon skeleton, active mass transfer is possible thus leading to a significant increase in the average crystallite size.

To obtain comprehensive information about nanostructure morphology of the obtained $YFeO_3$, microstructure features and results of crystallization processes TEM analyses of as-prepared and calcined samples were carried out (Fig. 3).

A significant difference between the morphology and microstructure is observed for the samples obtained from initial solutions with G/N ratio 2.4, 3.3 and 4.2. With decreased glycine to nitrate ratio, the pore size and pore wall thickness, on the contrary, increase. Comparing this information with data about phase and disperse composition of the samples (Table 2) it can be assumed that spatial restrictions may also affect the result of the glycine-nitrate combustion in addition to the combustion reaction zone temperature factor [26]. In this case, the phase and disperse composition of glycine-nitrate combustion products are not only strongly dependent on reaction temperature, but also on the combustion reaction rate and the amount of evolved gases, so that all these factors govern final product microstructure. However, as it seen after

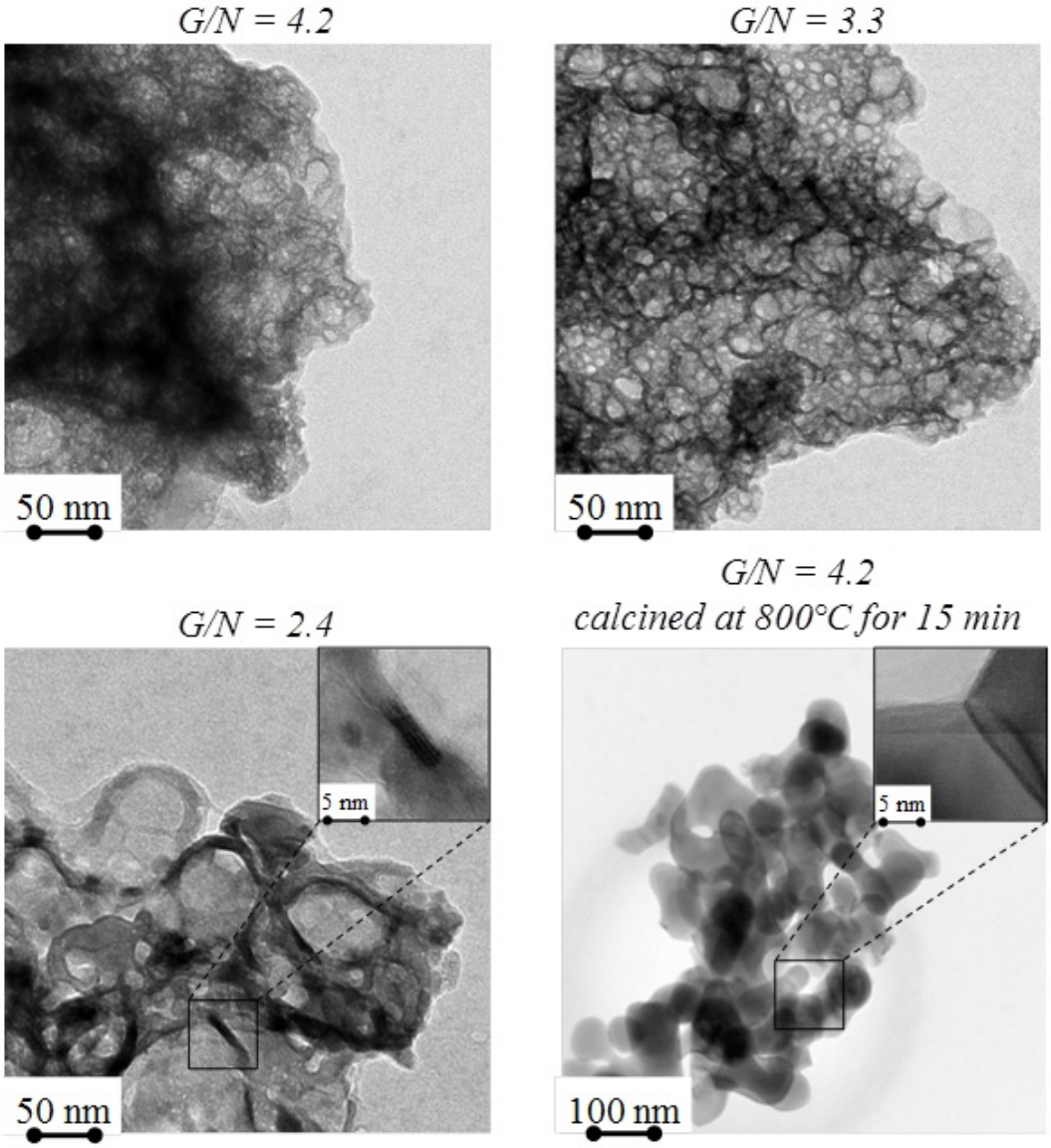

FIG. 3. TEM of glycine-nitrate combustion products as prepared ($G/N = 2.4$, 3.3, 4.2) and after heat treatment ($G/N = 4.2$, calcined 800 °C, 15 min)

the heat treatment, the initial microstructure of the composite is disrupted and orthorhombic orthoferrite is present as weakly agglomerated nanoparticles with rounded shapes. Apparently, nanoparticles o-$YFeO_3$ are formed on the base of the previous pore walls in the areas with enhanced congestion of initial substance.

This assumption is also confirmed by matching results of both helium pycnometry analysis and analysis of nitrogen adsorption with using average wall thickness equation as described above. Results of these calculations and scheme of morphological and phase changes depending on the G/N ratio is shown in Fig. 4.

The products of glycine-nitrate combustion have a porous structure and can be characterized by the average wall thickness of pores, which depends on the G/N ratio. The minimum wall thickness was detected at a glycine/nitrate ratio of about 3.0 – 3.3. If G/N ratio is 4.2 and 2.4, the average wall thicknesses of pores are maximized, but the reasons for this increase in

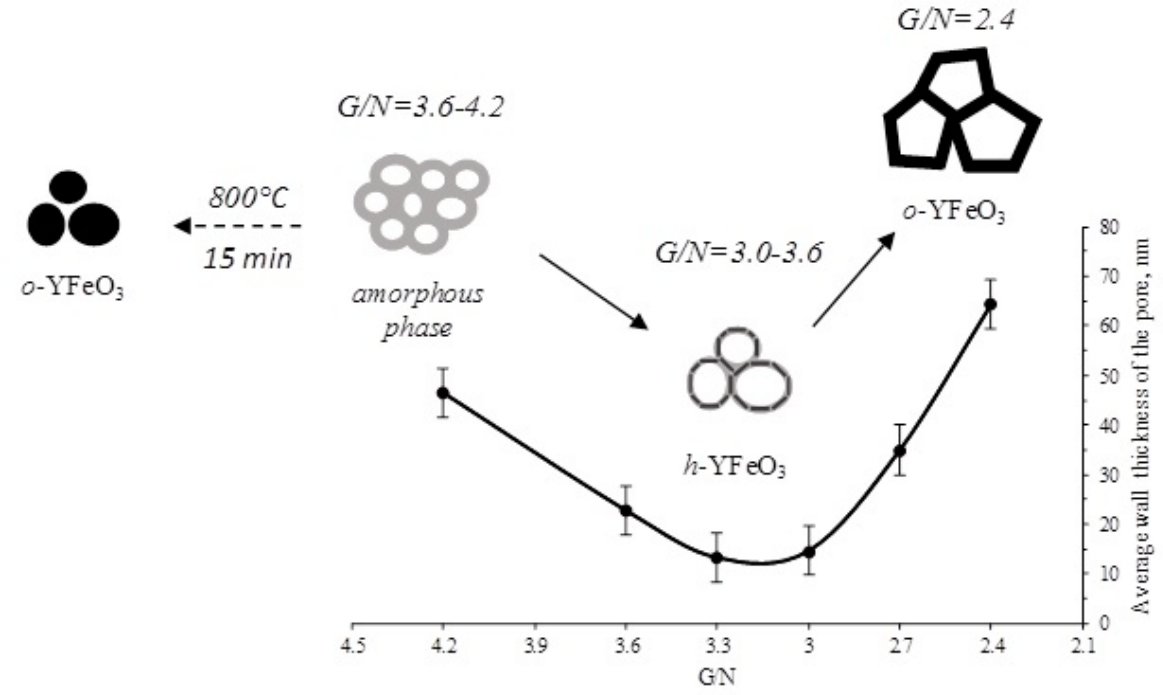

FIG. 4. Average wall thickness of the pores in glycine-nitrate combustion products at different G/N ratio and its phase and morphological transformation scheme

thicknesses are different. In the case of glycine excess ($G/N = 3.6 - 4.2$), the pore thickness is comparatively high mainly due to their structure formation from the abundance of unreacted substances. This leads to significant wall thickening, a reduction in the density of the sample, the formation of closed porosity and as a result, the foam morphology illustrated in Fig. 4. Otherwise, in the case of a decreased G/N ratio, in the range of 3.0 – 3.6, at the onset of crystallization processes, changes in the pore wall thickness and the morphology of the combustion products are observed, presumably due to the reduction of unreacted product amount. The sample obtained under minimal G/N ratio of 2.4 is characterized by maximal pore wall thickness due to its high crystallinity and high average crystallite size of $YFeO_3$. In this case, it is proper to consider nanostructure of the sample as fused plate-like structure, which is shown in Fig. 3. This assumption can be proved by comparing nanostructure average characteristic sizes estimated from XRD and TEM (Table 3). Average characteristic size of nanostructure refers to average wall thickness of the pores (TEM) or average crystallite size estimated from diffraction line broadening in different crystallographic directions (XRD).

Thus, it was shown a strong influence of unreacted combustion products on the morphology of obtained samples.

4. Conclusion

Nanostructured materials, based on the orthorhombic and hexagonal yttrium orthoferrite with different phase, disperse and morphological compositions, were obtained by direct glycine nitrate synthesis. It was shown that the composite morphology is strongly dependent upon the amount of evolved gases amounts and mass fraction of unreacted combustion products. Crystallization behavior of composites with different G/N ratio was shown mainly to depend on the reaction zone temperature as well as on spatial restrictions formed by the morphology

TABLE 3. Average characteristic sizes of nanostructures (from XRD and TEM) depending on synthesis conditions

G/N	Phase composition	Nanostructure average characteristic size, nm					
		XRD					TEM
		o-$YFeO_3$			*h*-$YFeO_3$		
		[200]	[002]	[040]	[010]	[004]	
4.2	Amorphous phase	–	–	–	–	–	> 40
3.3	*o*-$YFeO_3$ + *h*-$YFeO_3$	29±2	29±2	33±3	10±2	7±2	10 – 20
2.4	*o*-$YFeO_3$	46±4	46±4	51±5	–	–	15 – 50
4.2*	*o*-$YFeO_3$	50±5	49±5	51±5	–	–	> 50

* – the sample obtained by calcination of combustion products at 800 °C for 15 minutes

features and that leads to preferred formation of yttrium orthoferrite with amorphous, hexagonal or orthorhombic structures. As result of this work, a scheme for the morphological changes has been shown to be dependent upon the glycine to nitrate ratio.

Acknowledgments

This work was financially supported by the Russian Foundation for Basic Research (Project 13-03-12470).

References

[1] Chick L.A., Pederson L.R., et al. Glycine-nitrate combustion synthesis of oxide ceramic powders. *Mater. Lett.*, 1990, **10** (1–2), P. 6–12.
[2] Patil K.C., Aruna S.T., Mimani T. Combustion synthesis: an update. *Curr. Opin. Solid State Mater. Sci.*, 2002, **6**, P. 507–512.
[3] Mukasyan A.S., Epstein P., Dinka P. Solution combustion synthesis of nanomaterials. *Proc. Combust. Inst.*, 2007, **31** (2), P. 1789–1795.
[4] Aruna S.T., Mukasyan A.S. Combustion synthesis and nanomaterials. *Curr. Opin. Solid State Mater. Sci.*, 2008, **12** (3–4), P. 44–50.
[5] Saket S., Rasouli S., et al. Solution Combustion Synthesis of Nano-Crystalline Alumina Powders. *J. Mater. Sci. Eng.*, 2010, **4** (8), P. 80–84.
[6] Zhuravlev V.D., Vasil'ev V.G., et al. Glycine-nitrate combustion synthesis of finely dispersed alumina. *Glas. Phys. Chem.*, 2010, **36** (4), P. 506–512.
[7] Zhuravlev V.D., Bamburov V.G., et al. Solution combustion synthesis of α–Al_2O_3 using urea. *Ceram. Int.*, 2013, **39** (2), P. 1379–1384.
[8] Verma A., Dwivedi R., et al. Microwave-Assisted Synthesis of Mixed Metal-Oxide Nanoparticles. *J. Nanoparticles*, 2013, **2**, P. 1–11.
[9] Nair S.R., Purohit R.D., et al. Role of glycine-to-nitrate ratio in influencing the powder characteristics of La(Ca)CrO_3. *Mater. Res. Bull.*, 2008, **43** (6), P. 1573–1582.
[10] Chiu T.-W., Yu B.-S., et al. Synthesis of nanosized $CuCrO_2$ porous powders via a self-combustion glycine nitrate process. *J. Alloys Compd.*, 2011, **509** (6), P. 2933–2935.
[11] Jiang L., Liu W., et al. Rapid synthesis of $DyFeO_3$ nanopowders by auto-combustion of carboxylate-based gels. *J. Sol-Gel Sci. Technol.*, 2011, **61** (3), P. 527–533.
[12] Kondakindi R.R., Karan K., Peppley B.A. A simple and efficient preparation of $LaFeO_3$ nanopowders by glycine-nitrate process: Effect of glycine concentration. *Ceram. Int.*, 2012, **38** (1), P. 449–456.

[13] Komlev A.A., Vilezhaninov E.F. Glycine-nitrate combustion synthesis of nanopowders based on nonstoichiometric magnesium-aluminum spinel. *Russ. J. Appl. Chem.*, 2013, **86** (9), P. 1344–1350.
[14] Jose R., James J., John A.M., et al. A new combustion process for nanosized $YBa_2ZrO_{5.5}$ powders. *Nanostructured Mater.*, 1999, **11** (5), P. 623–629.
[15] Reddy B.M., Reddy G.K., Rao K.N., et al. Characterization and photocatalytic activity of TiO_2–M_xO_y (M_xO_y = SiO_2, Al_2O_3, and ZrO_2) mixed oxides synthesized by microwave-induced solution combustion technique. *J. Mater. Sci.*, 2009, **44** (18), P. 4874–4882.
[16] Khetre S.M., Jadhav H.V., Jagadale P.N., et al. Studies on electrical and dielectric properties of $LaFeO_3$. *Adv. Appl. Sci. Res.*, 2011, **2** (4), P. 503–511.
[17] Tien N.A., Almjasheva O.V., Mittova I.Ya., et al. Synthesis and magnetic properties of $YFeO_3$ nanocrystals. *Inorg. Mater.*, 2009, **45** (11), P. 1304–1308.
[18] Gil D.M., Navarro M.C., Lagarrigue M.C., et al. Synthesis and structural characterization of perovskite $YFeO_3$ by thermal decomposition of a cyano complex precursor, $Y[Fe(CN)_6]\cdot 4H_2O$. *J. Therm. Anal. Calorim.*, 2010, **103** (3), P. 889–896.
[19] Tang P., Chen H., Cao F., et al. Magnetically recoverable and visible-light-driven nanocrystalline $YFeO_3$ photocatalysts. *Catal. Sci. Technol.*, 2011, **1** (7), P. 1145–1148.
[20] Zhang R.L., Fang C., Yin W., et al. Dielectric behavior of hexagonal and orthorhombic $YFeO_3$ prepared by modified sol-gel method. *J. Electroceramics*, 2014, **32**, P. 187–191.
[21] Popkov V.I., Almjasheva O.V. Formation Mechanism of $YFeO_3$ Nanoparticles under the Hydrothermal Conditions. *Nanosyst.: Phys., Chem., Math.*, 2014, **5** (5), P. 703–708.
[22] Tugova E.A., Karpov O.N. Nanocrystalline Perovskite-Like Oxides Formation in Ln_2O_3–Fe_2O_3–H_2O (Ln = La, Gd) Systems. *Nanosyst.: Phys., Chem., Math.*, 2014, **5** (6), P. 854–860.
[23] Popkov V.I., Almjasheva O.V., Schmidt M.P., et al. Formation mechanism of nanocrystalline yttrium orthoferrite under heat treatment of the coprecipitated hydroxides. *Russ. J. Gen. Chem.*, 2015, **85** (6), P. 1370–1375.
[24] Wu L., Yu J.C., Zhang L., et al. Selective self-propagating combustion synthesis of hexagonal and orthorhombic nanocrystalline yttrium iron oxide. *J. Solid State Chem.*, 2004, **177** (10), P. 3666–3674.
[25] Zhang W., Fang C., Yin W., et al. One-step synthesis of yttrium orthoferrite nanocrystals via sol-gel autocombustion and their structural and magnetic characteristics. *Mater. Chem. Phys.*, 2013, **137** (3), P. 877–883.
[26] Popkov V.I., Almjasheva O. V. Yttrium orthoferrite $YFeO_3$ nanopowders formation under glycine-nitrate combustion conditions. *Russ. J. Appl. Chem.*, 2014, *87* (2), P. 167–171.
[27] Popkov V.I., Almjasheva O.V., Gusarov V.V. The investigation of the structure control possibility of nanocrystalline yttrium orthoferrite in its synthesis from amorphous powders. *Russ. J. Appl. Chem.*, 2014, **87** (10), P. 1417–1421.
[28] Popkov V.I., Almjasheva O.V., Schmidt M.P., et al. Features of Nanosized $YFeO_3$ Formation under Heat Treatment of Glycine-Nitrate Combustion Products. *Russ. J. Inorg. Chem.*, 2015, **60** (10), P. 1193–1198.
[29] Young R.A. *The Rietveld Method*. Oxford Univ. Press., Oxford, 1993, 312 p.
[30] Patterson A. The Scherrer formula for X-ray particle size determination. *Phys. Rev.*, 1939, **56**, P. 978–982.
[31] Goldstein J.I., Newbury D.E., Echlin P., et al. *Scanning Electron Microscopy and X-ray Microanalysis*. Springer, New York, 2003, 690 p.